

5-D Seismic Data Interpolation by Continuous Representation

Dawei Liu^{ID}, Wenbin Gao^{ID}, Weiwei Xu^{ID}, Ji Li^{ID}, Xiaokai Wang^{ID}, Member, IEEE, and Wenchao Chen^{ID}

Abstract—How to represent a seismic wavefield? Traditionally, while seismic wavefields are conceptualized continuously, acquisition geometries capture seismic data discretely using 2-D spatial coordinates. Motivated by recent advances in neural radiance fields for 3-D reconstruction through implicit neural representation, we introduce implicit seismic representation (ISR) for 5-D seismic data interpolation. This approach processes seismic data coordinates as inputs and outputs amplitude values at those coordinates with multilayer perceptrons (MLPs). Due to the continuous nature of the coordinates, ISR can achieve representations at any desired resolution and is easily scalable to a 5-D representation. To achieve a continuous representation of seismic data, we employ a self-supervised learning strategy to train the ISR on observed data. The trained network is then capable of interpolating missing seismic traces by querying every coordinate of the missing data. Our approach’s effectiveness is validated through synthetic and field data experiments, showcasing superior reconstruction abilities. Our findings highlight the potential of the implicit neural representation framework to achieve precise parametrization of continuous seismic wavefields, marking a significant advancement in seismic data processing and analysis.

Index Terms—5-D seismic reconstruction, continuous wavefield representation, implicit neural representations, parametrization, self-supervised learning.

I. INTRODUCTION

SEISMIC reconstruction algorithms recover missing traces due to difficult field operations and resource constraints, aiming to simultaneously interpolate and denoise seismic data. They play an indispensable and challenging role in improving the data quality for subsequent processing and interpretation, such as denoising [1], [2], [3], resolution enhancement [4], [5], and fault detection [6]. Consequently, seismic reconstruction is garnering increased attention.

Manuscript received 20 February 2024; revised 8 July 2024; accepted 16 July 2024. Date of publication 19 July 2024; date of current version 8 August 2024. This work was supported in part by the National Key Research and Development Program of China under Grant 2021YFA0716903, in part by the National Natural Science Foundation of China under Grant 42374135 and Grant 41974131, and in part by the Fundamental Research Funds for the Central Universities under Grant xzy012023073. (*Corresponding author: Wenchao Chen*.)

Dawei Liu is with the School of Information and Communications Engineering, Xi'an Jiaotong University, Xi'an 710049, China, and also with the Department of Physics, University of Alberta, Edmonton, AB T6G 2E1, Canada (e-mail: liudawei2015@stu.xjtu.edu.cn).

Wenbin Gao, Weiwei Xu, Xiaokai Wang, and Wenchao Chen are with the School of Information and Communications Engineering, Xi'an Jiaotong University, Xi'an 710049, China (e-mail: 1816364944@qq.com; 544274644@qq.com; xkwang@xjtu.edu.cn; wenchchen@xjtu.edu.cn).

Ji Li is with the Department of Geoscience, University of Calgary, Calgary, AB T2N 1N4, Canada (e-mail: li.ji1@ucalgary.ca).

Digital Object Identifier 10.1109/TGRS.2024.3431439

Seismic reconstruction is a classic example of an inverse problem characterized by its underdetermined nature, where multiple outputs could correspond to a single input. Traditional interpolation techniques use mathematical models to estimate missing values, leveraging structural relationships among the existing data points. These methods typically rely on assumptions, such as predictability, sparsity, and low rank. Predictability for linear events is a common approach, exemplified by the prediction error filter in the f - x domain [7], [8], [9], t - x [10] domain, and the f - k domain [11]. While effective, these methods necessitate manual tuning of parameters, such as filter length and window size, to align with the assumption of linear events. To accommodate more complex structures, certain transformations act as dictionaries to more closely match seismic data. Improved matching results in sparse coefficients within specific transformation domains, such as Radon [12], [13], [14], Shearlet [15], Seislet [16], [17], and curvelet [18], [19], [20] domains. By enforcing sparsity in the transform domain, they gradually recover missing traces that conform to predefined structures through optimization iterations. However, these methods can be computationally demanding and highly sensitive to threshold parameter selection, making them challenging for high-dimensional problems. Rank-reduction methods presuppose that incomplete data and noise elevate the rank of seismic data. According to different rank definitions, they can be categorized into matrix-based and tensor-based approaches. Tensor-based methods often surpass matrix-based ones by exploiting more coherent structures across various dimensions. This demonstrates the advantage of effectively utilizing all physical dimensions of the original seismic wavefield, thereby encouraging scholars to pursue further advancements in this direction.

Due to memory constraints, conventional methods for processing large 5-D datasets typically involve segmenting the data into smaller patches and then stitching them back together after processing. They effectively capture local features within each sliding patch. However, it has a significant drawback: the inability to model global structural similarities across patches. Since each segment is processed in isolation without interpatch communication, multidimensional consistency and reconstruction accuracy may be compromised.

Conversely, supervised deep learning, a recent area of intense interest, excels at characterizing global features despite cropped training patches. It offers a more adaptive interpolation strategy. The critical difference lies in the loss function, which encompasses all patches, enabling the model to learn

complex nonlinear relationships incrementally from a comprehensive training dataset [21]. Furthermore, supervised learning circumvents the arduous task of designing handcrafted priors by employing end-to-end training, which allows for a more flexible learning process. Consequently, numerous supervised deep learning models have been applied to seismic data reconstruction [22], [23], [24], [25]. However, a significant challenge for supervised learning is constructing high-quality labels, as acquiring a large and diverse training dataset is challenging and labor-intensive. Using conventional methods to generate labels is effective but may result in a network whose performance mirrors the labels, without clear superiority. Labels created through forward modeling are often highly accurate but require geological expertise. Inaccurate geological knowledge may lead to generalization issues when applied to real-world data. Moreover, most supervised methods operate in 2-D or 3-D due to GPU memory limitations, leaving ample room for direct 5-D modeling to enhance performance. One promising approach to capturing the inherent structure of 5-D data involves constructing a pseudo-5-D convolution by cascading a 3-D convolution operator with a 2-D convolution [26]. Despite this advancement, the approach still suffers from high-computational costs, which limits its applicability to large-scale 5-D prestack datasets in practical scenarios.

To mitigate label restrictions, researchers seek solutions from self-supervised methods. In contrast to conventional techniques that rely on predetermined formulas, self-supervised deep learning methods adapt dynamically to the unique features of each dataset by exploiting the inherent structure and patterns, potentially leading to superior reconstruction quality. Methods based on deep image priors have been successfully employed for seismic interpolation [27], [28]. However, they are not without their challenges, such as instability due to early stopping and the risk of overfitting to noise or artifacts. This instability further impedes its ability to integrate seamlessly with various regularization techniques, thereby reducing its adaptability. Masked modeling [29], a technique in self-supervised learning, has also been adapted for seismic interpolation [30], [31], [32]. While promising, their effectiveness depends heavily on data quality. This is a concern for 5-D prestack seismic data, which is often contaminated by various types of noise. In addition, the high rate of missing traces in raw 5-D seismic datasets hinders us from further decimating the data to create paired training sets. The computationally intensive nature of training and deploying high-dimensional networks remains a significant barrier, preventing current unsupervised methods from scaling to higher dimensions. Therefore, there is a pressing need for an innovative interpolation method capable of harnessing 5-D features in a global context. To be viable, such a method must not rely on labeled data. Moreover, considering the sheer volume of 5-D prestack data, the method should employ a lightweight network architecture to address computational challenges. Ideally, it would also incorporate noise attenuation capabilities, adding further value to the technique.

Continuous neural representations have recently emerged as a powerful and flexible alternative to classical discretized signal representations. One notable example is the neural

radiance field [33], [34], [35], [36], which utilizes continuous representation to achieve remarkable progress in 3-D scene reconstruction. This success prompts an intriguing inquiry: “can continuous representation directly interpolate 5-D data?” To address this, we leverage the adaptability of self-supervised learning to propose an effective and efficient method for 5-D seismic data interpolation, namely, implicit seismic representation (ISR). Our approach integrates continuous representation into 5-D data interpolation, achieving superior performance. Specifically, the ISR network takes any 5-D coordinates as input and outputs the corresponding amplitude value. Network training aims to induce the neural network to overfit a specific dataset, learning its intrinsic properties. In essence, ISR embeds the 5-D continuous wavefield into the network weights. Due to its pixelwise training strategy, ISR exhibits efficient GPU memory usage compared with the existing convolutional networks. During the inference phase, the network is queried at each 5-D coordinate requiring interpolation, thereby achieving 5-D seismic reconstruction. We evaluate the effectiveness of ISR using synthetic data and demonstrate the robustness of our model with a corrupted field dataset. These findings underscore ISR’s potential as an innovative solution for 5-D seismic data interpolation, paving the way for more precise and efficient continuous seismic wavefield representation.

The article is structured as follows. Section II outlines the 5-D interpolation task and details the implicit regularization for continuous representation. Subsequently, the ISR method for 5-D seismic interpolation is introduced. Section III showcases the reconstruction results from experiments on synthetic and field seismic data, demonstrating the effectiveness of the proposed technique. Section IV discusses limitations and future directions. Finally, the conclusion is presented in Section V.

II. METHOD

A. 5-D Interpolation Formulation

Five-dimensional seismic data acquisition enhances traditional seismic data acquisition by incorporating two additional dimensions—often offset and azimuth, enabling a more detailed capture of subsurface structures [37]. This approach provides a more comprehensive understanding of the seismic wavefield by capturing seismic response variations across different azimuths and offsets. The resulting 5-D dataset offers profound insights into the subsurface through improved spatial sampling, which leads to more accurate reservoir identification and property evaluation. However, reconstructing 5-D seismic data presents a considerable challenge, primarily due to the vast amount of data required for precise representation of subsurface structures. The wide-azimuth nature of the data necessitates an interpolation approach that concurrently utilizes information from all spatial dimensions, as sampling along any specific subset of the four spatial dimensions is typically sparse. Consequently, sophisticated techniques are essential to handle the extensive data volume and effectively distill valuable insights.

As advanced linear algebra, tensors provide a discrete representation for received seismic wavefields. They align

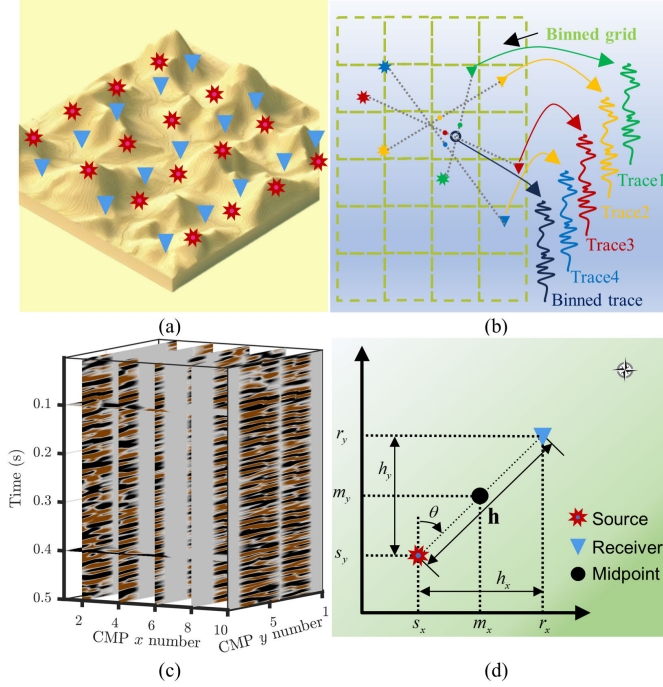


Fig. 1. Illustration of seismic exploration for 5-D data. (a) Seismic source and receiver layouts. (b) Schematics for data binning. (c) Three-dimensional subset of binned data. (d) Coordinate system used for describing the 5-D seismic data.

seismic data into a structured format with regularly spaced sampling grids. However, achieving this presents significant challenges in 5-D seismic acquisition due to the commonly irregular spatial arrangement of sources and receivers. Fig. 1(a) exemplifies a distribution of source and receiver. Each source is activated in sequence, with various receivers capturing the emitted signals simultaneously. Repeated activation facilitates multiple coverage of the work area, increasing data accuracy. To reconcile the irregularly sampled data with tensor representation requirements, a binning process is employed, as depicted in Fig. 1(b). This critical step groups seismic traces into distinct hypercubes based on common midpoint (CMP) positions. Subsequently, the traces within each hypercube are averaged to yield a single representative trace. Binned data often exhibit significant missing traces, a challenge graphically illustrated in Fig. 1(c), underscoring the imperative for sophisticated data interpolation techniques. Following the binning procedure, the seismic dataset is transformed into a poststack format via the CMP gather stacking method. This technique amalgamates multiple CMP records corresponding to identical midpoint locations, thereby enhancing data quality. The final stages encompass additional processing and migration to improve the imaging of underground geological structures.

Various data types emerge accordingly during the extensive process of seismic data manipulation. For instance, entries in the observed source-receiver coordinates can be represented as the tensor $\mathcal{D}^{\text{obs}}(t, s_x, s_y, r_x, r_y)$, where (s_x, s_y, r_x, r_y) delineates the spatial coordinates of sources and receivers. An alternative sorting schema denotes the entries as $\mathcal{D}^{\text{obs}}(t, m_x, m_y, h_x, h_y)$, t denotes time, m_x and m_y indicate the inline and crossline midpoint coordinates,

and h_x and h_y represent inline and crossline offsets. In yet another arrangement, the data may be ordered as $\mathcal{D}^{\text{obs}}(t, m_x, m_y, |\mathbf{h}|, \alpha)$, with $|\mathbf{h}|$ signifying the offset distance and α representing the azimuth. Without loss of generality, we state that \mathbf{v} represents the coordinates of a single data point within our source-receiver coordinates. Specifically, $\mathbf{v} = [v_1, v_2, v_3, v_4, v_5]^T$ is a single 5-D coordinate sample selected from the regular coordinate set \mathcal{V} . This general designation simplifies notations and provides a fundamental basis for further analysis across various types of seismic data.

With the above mathematical notations, we can describe the relationship between the observed decimated data \mathcal{D}^{obs} and the corresponding complete data \mathcal{Z} as follows:

$$\mathcal{D}^{\text{obs}} = \mathcal{P}(\mathcal{Z}) \quad (1)$$

where \mathcal{P} is a sampling operator that retains values at coordinates \mathbf{v} with observed data and assigns a zero elsewhere. Building on this, we define a cost function to reconstruct the unknown data

$$\min E(\mathcal{D}^{\text{obs}}, \mathcal{P}(\mathcal{Z})) + \alpha \mathcal{R}(\mathcal{Z}) \quad (2)$$

where $E(\cdot, \cdot)$ is a data fitting metric, which ensures that the model accurately reflects \mathcal{Z} and aligns closely with the observed data. The regularization term $\mathcal{R}(\mathcal{Z})$ is added to the loss function to prevent overfitting by penalizing complex models. It encourages the model to be simpler, which can lead to better generalization on unseen data. Note that regularization can be explicit, like ℓ_1 and ℓ_2 regularization, or implicit, like early stopping, data augmentation, and architecture adjustments. The coefficient α serves to balance the data fitting metric with the regularization term. An overemphasis on data fitting leads to overfitting, causing the model to learn noise rather than the underlying distribution of desired reflections. On the other hand, prioritizing regularization excessively may result in underfitting, making the model too simple to capture the complexity of the useful data. Thus, fine-tuning α is essential for achieving an accurate and generalizable model.

B. Continuous Neural Representations as an Implicit Regularizer

Multilayer perceptrons (MLPs) are effective in learning continuous functions compared with the localized receptive fields of convolutional neural networks. Accordingly, continuous neural representations employ an MLP, denoted as $\phi_{\theta}(\mathbf{v}) : \mathbb{R}^d \mapsto \mathbb{R}^o$, to approximate the explicit solution of an implicit function $F(\mathbf{v}, \phi_{\theta}, \nabla_{\mathbf{v}}\phi_{\theta}, \nabla_{\mathbf{v}}^2\phi_{\theta}, \dots) = 0$. For instance, a seismic dataset $\mathcal{Z} \in \mathbb{R}^{V_1 \times V_2 \times V_3 \times V_4 \times V_5}$ can be represented with $\phi_{\theta}(\mathbf{v}) : \mathbb{R}^5 \mapsto \mathbb{R}$, which follows the condition $\phi_{\theta}((v_1/V_1), (v_2/V_2), (v_3/V_3), (v_4/V_4), (v_5/V_5)) = \mathcal{Z}_{v_1 v_2 v_3 v_4 v_5}$, for $v_i \in \{1, \dots, V_i\}$, $i = 1, 2, \dots, 5$. Here, v_i denotes the index in the i th dimension, which encompasses V_i discrete sampling points. Unlike traditional discretized representations, the detail captured by continuous neural representations is not limited by the grid resolution v_1, v_2, v_3, v_4 , and v_5 , as it can predict values at any location $\mathbf{v} \in \mathbb{R}^5$, not just at discrete intervals, such as $((v_1/V_1), (v_2/V_2), (v_3/V_3), (v_4/V_4), (v_5/V_5))$. In addition, scaling to higher dimensions is straightforward by increasing

the dimensionality of \mathbf{v} . This property is particularly beneficial to large-scale applications, freeing us from constructing high-dimensional operators. The continuous neural representation encodes data in the weights of a neural network rather than storing it explicitly, leading to a dramatic reduction in memory requirements. Therefore, it has gained widespread use in machine learning for view synthesis [38], [39], [40], signal compression [39], [41], and classification [42].

Continuous neural representations are increasingly recognized as an effective implicit regularizer in image restoration [43], [44]. This stems from an intriguing paradox that modern deep neural networks, although highly overparameterized compared with training data, often generalize well beyond classical statistical expectations [45]. This ability enables them to capture the essence of natural data. Initial theoretical explanations began with simple linear neural network models, analyzing them through the lens of gradient dynamics. Continuous form (infinitesimally small) of gradient dynamics made some theoretical progress, which indicates that implicit regularization favors low-rank solutions [46], [47], [48]. Razin et al. [49] stepped further toward practical deep learning and provide theoretical analysis of this implicit regularization in tensor form via certain type of nonlinear neural networks, suggesting a bias toward lower complexity in representations. The tendency toward low rank or simpler representations is, thus, extended from matrices (2-D arrays) to tensors (multidimensional arrays). However, the above continuous form of gradient dynamics deviates from actual applications, since the practical learning rate is usually noninfinitesimal. Further exploration has led to the development of discrete gradient dynamics [50], [51], [52] to bridge the gap between theoretical propositions and practical implementation constraints. However, this theory imposes a computational tax for trajectory analysis and has primarily been explored within the confines of simpler, two-layer networks.

Alternatively, some researchers turn to Fourier spectrum analysis and theoretically prove that coordinate-based MLPs have the nature of “spectral bias” [53], [54], [55]. They highlight that the networks exhibit an inherent preference for lower frequency functions. This bias acts as a built-in filter against high-frequency noise, prioritizing smoother functions over more erratic ones. Valle-Pérez et al. [56] also provided clear evidence that deep nonlinear networks have a strong simplicity bias toward simple Boolean functions. Despite the ongoing evolution of theoretical analysis, low-rank, spectral, and simplicity biases have demonstrated their utility in refining neural network models to more accurately capture and represent continuous signals as an effective regularizer.

C. 5-D Seismic Interpolation by ISR

Leveraging the regularization introduced by continuous neural representations, we implement ISR to interpolate 5-D seismic data by encapsulating the continuous nature of the seismic 5-D wavefield. We adopt the square function as our data fitting metric E for its simplicity, and the 5-D ISR interpolation can be formulated as $F(\theta, \mathbf{v}, \mathcal{D}^{\text{obs}}) =$

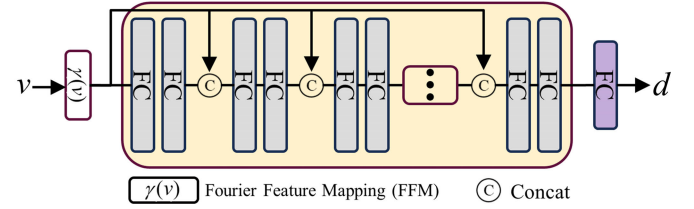


Fig. 2. Network architecture for the proposed ISR 5-D interpolation method.

$(\mathcal{P}(\phi_\theta(\mathbf{v})) - \mathcal{D}^{\text{obs}}(\mathbf{v}))^2 = 0$, where $\phi_\theta(\mathbf{v}) : \mathbb{R}^5 \rightarrow \mathbb{R}$ represents the model output and $\mathcal{D}^{\text{obs}}(\mathbf{v}) : \mathbb{R}^5 \rightarrow \mathbb{R}$ is the observed seismic dataset to be reconstructed. Note that our approach can easily extend to a higher dimension, such as time-lapse 5-D reconstruction. The 5-D ISR interpolation is formulated as follows:

$$\theta^* = \arg \min_{\theta} \sum_{(\mathbf{v}_i, d_i) \in \mathcal{V} \times \mathcal{D}^{\text{obs}}} (\mathcal{P}(\phi_\theta(\mathbf{v}_i)) - d_i)^2 \quad (3)$$

where $d_i = \mathcal{D}^{\text{obs}}(\mathbf{v}_i)$ is the i th observed sampling point corresponding to the normalized coordinate $\mathbf{v}_i = (v_{1i}, v_{2i}, v_{3i}, v_{4i}, v_{5i})$ and $\mathcal{V} \times \mathcal{D}^{\text{obs}} = \{(\mathbf{v}_i, d_i)\}_{i=1}^N$ is the training set. The training set is sampled from the regular grid of values from observed $\mathcal{D}^{\text{obs}} \in \mathbb{R}^{V_1 \times V_2 \times V_3 \times V_4 \times V_5}$. After training, $d(\mathbf{v})$ is predicted by $\phi_{\theta^*}(\mathbf{v})$ at any location \mathbf{v} .

The network architecture, depicted in Fig. 2, comprises a Fourier feature mapping (FFM) layer $\gamma(\mathbf{v})$ and a subsequent MLP $N_\theta : \gamma(\mathbf{v}) \mapsto d_i$, requiring optimization of parameters θ to conform with observed data. Alternatively, the network can be formalized as $\phi_\theta(\mathbf{v}) = N_\theta(\gamma(\mathbf{v}))$.

1) *Fourier Feature Mapping*: While standard MLPs are versatile approximators, they often struggle with high-frequency features. According to Tancik et al. [57], MLPs with the rectified linear unit (ReLU) activation function cannot effectively capture high-frequency components, and a Fourier feature encoder can significantly improve the representation ability of implicit neural representations. Inspired by this, ISR involves expanding input coordinates through a high-dimensional Fourier mapping $\gamma(\mathbf{v})$, significantly improving the model’s ability to discern high-frequency information. This Fourier spectrum expansion is defined by

$$\gamma_K(\mathbf{v}) = [\cos(\omega_1 v_1), \sin(\omega_1 v_1), \cos(\omega_1 v_2), \sin(\omega_1 v_2), \dots, \cos(\omega_K v_5), \sin(\omega_K v_5)]^\top \quad (4)$$

where K is the component count and ω_i reflects linear ($\omega_i = i\pi/2$) or exponential ($\omega_i = \pi 2^i$) frequency mappings, aiding in accelerated model convergence for seismic signals. We adopt an exponentially varying ω , because it proves more effective for seismic signals in our tests. In addition, despite seismic data having different coordinate lengths and units along different dimensions, it is not necessary to incorporate a composite encoding. While anisotropic encoding has proven beneficial in various applications, our experimental findings indicate that it does not provide added advantages for the specific tasks addressed in our research.

2) *MLP Architecture*: The architecture of MLP part N_θ consists of 17 fully connected (FC) layers. The first 16 layers each feature 256 hidden neurons and employ the ReLU

activation function, while the final layer comprises 128 hidden neurons and forgoes an activation function. Skip connections in MLPs can help with the vanishing gradient problem and enhance model accuracy [58], [59]. To bolster network training efficacy, we have integrated seven skip connections. These are strategically introduced after every second FC layer, terminating after the 16th layer, and serve to merge the initial input $\gamma(\mathbf{v})$ with the intermediate representation of N_θ .

The mathematical representation of MLP ϕ_θ with $L = 16$ layers is defined by the final output from the last layer

$$\phi_\theta(\mathbf{v}) = \mathbf{z}^{(L+1)} \quad (5)$$

where each layer ℓ , ranging from 1 to $L + 1$, computes the preactivation vector

$$\mathbf{z}^{(\ell)} = \mathbf{W}^{(\ell)} \mathbf{v}^{(\ell-1)} + \mathbf{b}^{(\ell)} \quad (6)$$

and, subsequently, the activation vector

$$\mathbf{v}^{(\ell)} = \sigma(\text{concat}(\mathbf{z}^{(\ell)}, \mathbf{s}^{(\ell)})). \quad (7)$$

Here, $\sigma(\cdot)$ is an elementwise ReLU activation function, and $\mathbf{v}^{(0)} = \gamma_K(\mathbf{v})$. The network parameters are denoted by $\theta = \{\mathbf{W}^{(\ell)}, \mathbf{b}^{(\ell)} \mid \ell = 1, 2, \dots, L + 1\}$, where $\mathbf{W}^{(\ell)} \in \mathbb{R}^{n_\ell \times n_{\ell-1}}$ and $\mathbf{b}^{(\ell)} \in \mathbb{R}^{n_\ell}$ define the weights and biases for each layer, respectively. The notation n_ℓ indicates the number of neurons in the ℓ th layer with $n_0 = 5$ and $n_{L+1} = 1$. The concatenation operation, denoted by $\text{concat}(\cdot, \cdot)$, merges the layer's output with the skip connection before activation, enriching the model's feature space and enhancing its ability to learn complex patterns. The skip connections are achieved by

$$\mathbf{s}^{(\ell)} = \begin{cases} \mathbf{v}^{(0)}, & \text{if } \ell \bmod 2 = 0 \\ 0, & \text{otherwise.} \end{cases} \quad (8)$$

The network's lightweight design ensures manageable training times per epoch, making it practical for seismic 5-D interpolation.

III. EXPERIMENTS

A. Synthetic Data Example 1

To assess the effectiveness of our continuous neural implicit representation for seismic data interpolation, we create a synthetic 5-D seismic dataset $\mathcal{G}(t, m_x, m_y, h_x, h_y)$ with the dimensions of $256 \times 20 \times 20 \times 10 \times 10$. This dataset features 20 samples per CMP dimension, ten traces per offset dimension, and 256 time samples per trace. For quantitative analysis, we introduce a reconstruction quality metric, Q , defined in decibels (dB) as follows:

$$Q [\text{dB}] = 10 \log_{10} \left(\frac{\|\mathcal{G}^{\text{true}}\|_F^2}{\|\mathcal{G}^{\text{true}} - \mathcal{G}^{\text{recon}}\|_F^2} \right) \quad (9)$$

where $\mathcal{G}^{\text{true}}$ represents the original complete data and $\mathcal{G}^{\text{recon}}$ denotes the reconstructed data.

To simulate real-world seismic data scenarios of incomplete seismic data, we randomly omit seismic traces by a sampling operator. In our experimental design, we remove 90.3% of seismic traces, resulting in a sparsely populated dataset, \mathcal{G}^{obs} . Subsequently, we employ the proposed ISR interpolation

method illustrated in Fig. 2 to reconstruct the missing seismic data.

In the FFM module, we set $K = 10$ for encoding each input coordinate, and the frequency ω varies exponentially. Unlike traditional methods that often use small sliding patches for processing 5-D seismic data, our network's ample capacity allowed us to encode the entire dataset \mathcal{G}^{obs} directly into the MLP during the self-supervised training phase. After training, we query the network for each coordinate point to determine its corresponding value.

Fig. 3 illustrates our experiment results, and we fix the inline and crossline offsets to $h_x = 2$ and $h_y = 2$, respectively. We extract 3-D cubes for visual comparison from the complete dataset $\mathcal{G}^{\text{true}}$, the decimated observed dataset \mathcal{G}^{obs} , and the reconstructed dataset $\mathcal{G}^{\text{recon}}$. As shown in Fig. 3(b) and (c), the ISR interpolation method achieves impressive results, almost perfectly recovering the missing traces. According to the Q metric, the quality of the reconstructed data relative to the original is as high as 39.83 dB, demonstrating the robustness and effectiveness of our proposed model in dealing with significant data sparsity.

B. Synthetic Data Example 2

To rigorously assess the reconstruction capabilities of our method on more complex wavefields, we conduct tests on an open-source 5-D seismic dataset available at https://wiki.seg.org/wiki/SEG_C3_NA. This dataset is composed of 51 sail lines, with each featuring 96 shots, eight streamers per shot, and 68 receivers per streamer. This results in a large total data volume of $625 \times 51 \times 96 \times 8 \times 68$. Each temporal sample is collected at an 8-ms interval, spanning 625 samples in the time dimension. Notably, the dataset is presented without normal moveout (NMO) correction, thus rendering a formidable challenge for any data reconstruction technique due to the unadjusted travel times with high curvatures.

For our experimental analysis, we concentrate on sail lines numbered 25–41, extracting a subset of data $\mathcal{O}(t, s_x, s_y, r_x, r_y)$ with the dimensions of $384 \times 16 \times 32 \times 8 \times 32$. We then subject this subset to manual decimation to examine the performance of the continuous neural implicit representation technique in interpolating 5-D seismic data. To emulate the common issue of missing traces in real-world seismic data, we apply a masking process that randomly omits seismic traces. In our experimental design, we intentionally removed 80% of the seismic traces, creating a highly sparse dataset \mathcal{O}^{obs} . This level of sparsity is representative of the challenges frequently faced in seismic data acquisition and processing, providing a stringent test bed for our interpolation methodologies.

Fig. 4 presents a comparative analysis of reconstruction results across eight gathers. The original data, depicted in Fig. 4(a), exhibit relatively horizontal events in shallow regions and dipping events at greater depths, with the variety of event features adding complexity to the interpolation task. The decimated data, shown in Fig. 4(b), are so sparse that the continuity of the original event structures is severely disrupted.

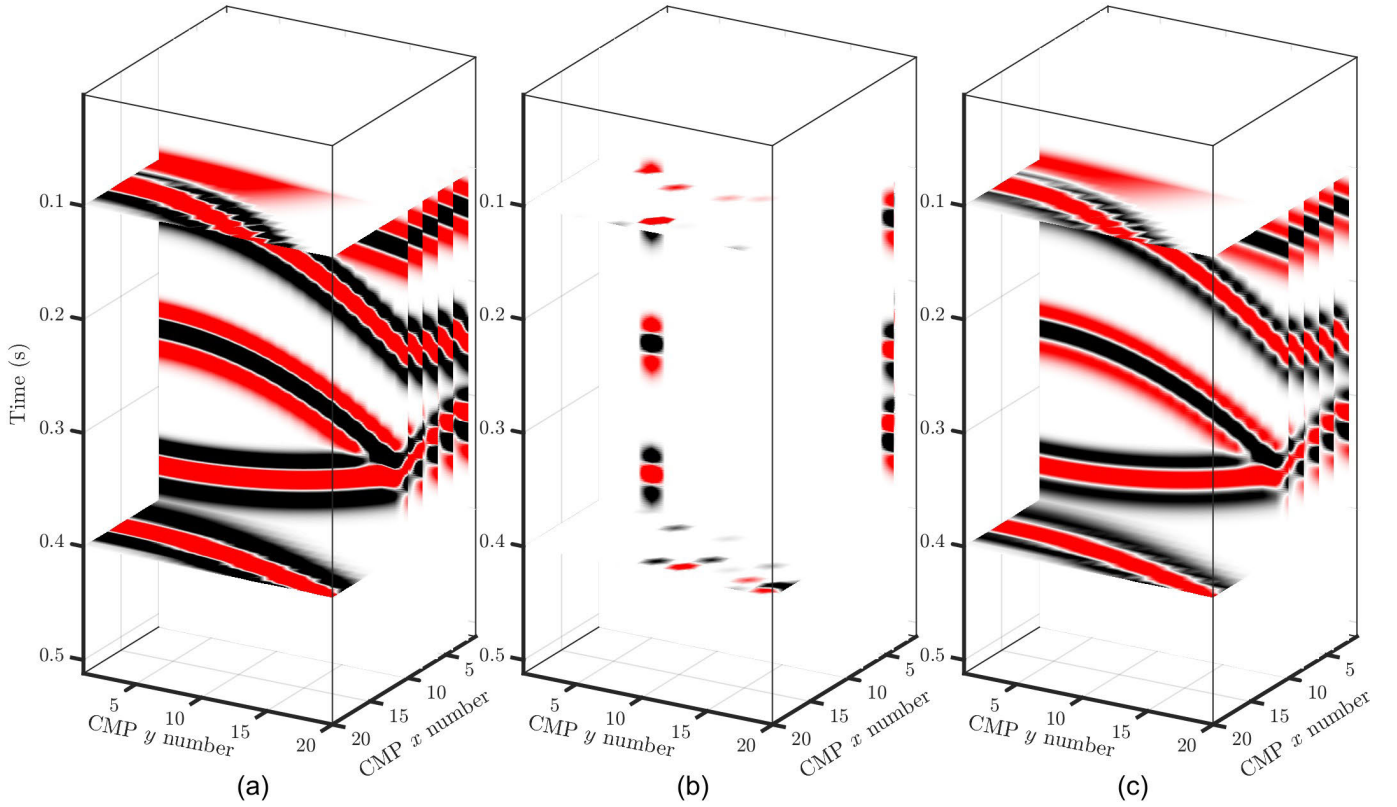


Fig. 3. (a) Three-dimensional slice view of noise-free synthetic 5-D complete data. (b) Decimated data with a missing rate of 90.3%. (c) Reconstructed results by the proposed ISR method.

As a benchmark, we selected an established damped rank-reduction (DRR) method [60]. This conventional approach, represented in Fig. 4(c), demonstrates proficiency in reconstructing seismic data. Nonetheless, it struggles with the reconstruction of deep-layer dipping events due to rapidly changing dips, which is a common limitation of traditional methods. Moreover, as DRR operates in the frequency domain, it inevitably introduces artifacts, particularly above the first arrivals. This issue is also evidenced in Fig. 4(d), where signal leakage is apparent.

Conversely, the reconstructed results from our proposed ISR method, displayed in Fig. 4(e), reveal a cleaner reconstruction with fewer artifacts than the DRR output. The ISR method also successfully recovers more intricate wavefield features within the deeper layers, showcasing a robust capability for complex feature extraction. The difference gathers, illustrated in Fig. 4(f), indicate that our method introduces less leakage.

For a quantitative comparison, we computed the Q value across the entire dataset $\mathcal{O}(t, s_x, s_y, r_x, r_y)$. Our ISR method outperforms the DRR method with a Q value of 12.88 dB compared with 11.34 dB. This substantial improvement underscores the superior learning and generalization ability of the ISR method in reconstructing a continuous 5-D wavefield, even in the presence of substantial data sparsity and complex geological scenarios. All the experimental parameters of our method are kept the same as in the previous example, demonstrating a flexible parameter selection that is robust across different datasets and interpolation challenges.

The DRR method is executed on an Intel¹ Core² i9-12900H CPU at 2.50 GHz, completing the task in 1444 s. Conversely, the ISR method uses an NVIDIA GPU 2080 Ti, which requires 890 min for training; however, its testing phase is significantly faster, taking only 600 s. Despite the considerable initial computational investment in training, the efficiency of the testing phase renders it practical for real-world applications. Our approach remains cost-effective in deep learning applications, as it utilizes simplified neural networks that are typically less resource-intensive. We will further recognize opportunities for reducing training costs by updating codes and GPUs, enhancing the overall efficiency of our method.

C. Field Data Experiment

Field data contrasts with synthetic data due to its inherent complexity and prevalent noise. These challenges pose significant difficulties for neural network training. To evaluate the robustness and efficacy of our proposed ISR methodology, we juxtapose it with the established DRR technique, utilizing a land dataset acquired in China for our comparative study. This dataset has been transformed from its irregularly sampled state into regular grids. It comprises 250 temporal samples at a 4-ms sampling interval, with ten midpoint x samples, ten midpoint y samples, 21 offset x samples, and ten offset y samples. The dataset is characterized by a 82% of its traces

¹Registered trademark.

²Trademarked.

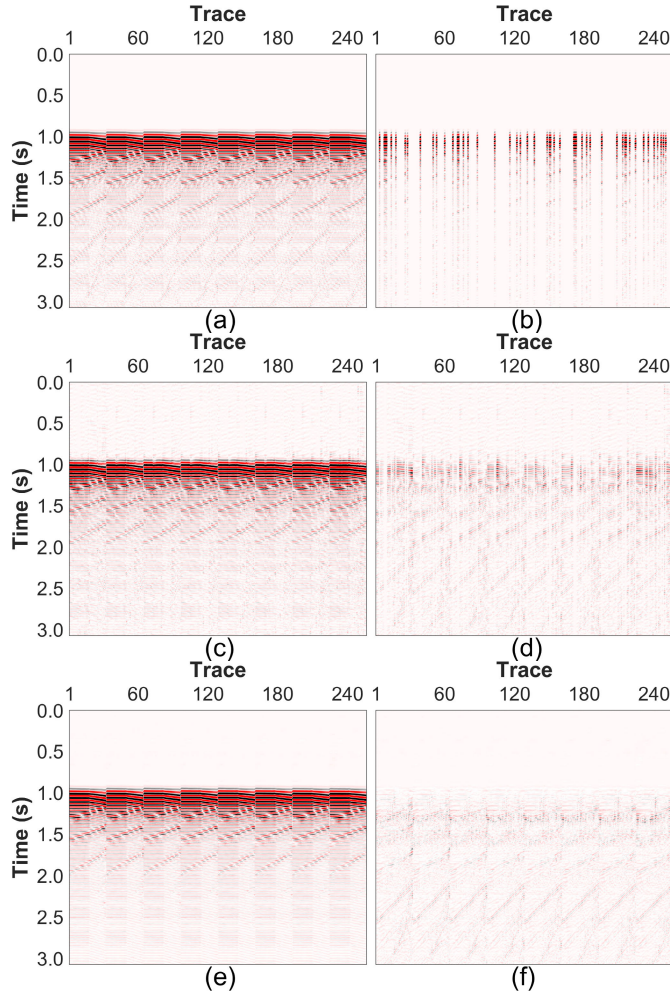


Fig. 4. Comparison of results obtained using different methods to reconstruct synthetic data. (a) Eight complete common receiver gathers obtained by fixing $s_x = 16$ and $r_y = 32$. (b) Decimated data with 80% traces irregularly missing. (c) and (d) Recovered results and reconstruction errors using the DRR method, respectively. (e) and (f) Recovered results and reconstruction errors using the proposed ISR method, respectively.

missing, presenting a formidable challenge for reconstruction algorithms.

Within Fig. 5(a), we illustrate a subset of original CMP gathers at CMP $x = 5$ and CMP $y = 5$. The data section is contaminated with substantial gaps, indicative of the challenges inherent in field data reconstruction. These data serve as the training target for our ISR method, as delineated in (3). For this dataset, our method still employs an exponential variation of the frequency ω and maintains the parameter $K = 10$ within the FFM module. This parameter choice aligns with the configurations used in our preceding experiments, ensuring consistency in our methodological approach across different datasets. Due to the prevalent noise, we apply a denoising step to the results obtained from both DRR and ISR by executing the DRR process once more, enhancing the outcome quality. The CMP section results obtained by DRR are displayed in Fig. 5(b), demonstrating effective recovery of the missing traces from Fig. 5(a). Despite this, some artifacts linger at the boundaries, partially obscuring valuable events as indicated by the yellow arrows. In Fig. 5(c), we present

the ISR results, which exhibit remarkable recovery of all missing traces, even in regions with significant data gaps. When compared with the DRR approach, our method yields better reconstruction quality, delineating clear and continuous events, particularly with enhanced clarity in the boundary regions. These findings underscore the proficiency of neural networks in modeling complex, high-dimensional data fields in a continuous manner.

To further substantiate the effectiveness of our ISR method, we maintain a fixed CMP y at 5 and an offset y at 5 for examining reconstruction quality across various dimensions. The original seismic data sections, shown in Fig. 6(a), are severely affected by numerous missing traces and noise. Fig. 6(b) and (c) delineates the outcomes of the DRR and ISR methods, respectively. It is apparent that the ISR method excels at recovering the missing traces, indicating that the network has effectively captured the essence of the intrinsic 5-D seismic wavefield. While both methods achieve commendable results in Fig. 6, the ISR method exhibits superior lateral consistency in the reconstructed reflections, as black arrows indicate, suggesting that the employed MLP model naturally favors smooth interpolations among data points. Moreover, the yellow arrows highlight the previous observation that ISR enhances signal energy at boundaries. Consistent with the regularizer analysis in Section II-B, ISR not only enhances horizontal continuity in the reconstructed data but also demonstrates greater resilience to noise during the interpolation process.

Although we are constrained to present only a fraction of the field data and our discussion is limited to the observed performance, the stacking results offer a comprehensive comparative analysis. Fig. 7(a) showcases the stacked data prior to interpolation, where a noisy time slice is evident in the shallow-layer regions. The stacked cubes reconstructed using the DRR and ISR methods, as depicted in Fig. 7(b) and (c), respectively, markedly mitigate prestack noise and amplify the signal energy relative to the original stack in Fig. 7(a). Nonetheless, the profiles in Fig. 7(b) still reveal minor residual noise in the shallow layers. In contrast, the profiles in Fig. 7(c) exhibit a minimal level of random noise, attesting to the superior noise resistance capabilities of the ISR method. This stacking comparison effectively demonstrates the enhanced performance of our ISR method over traditional rank-reduction techniques in 5-D field data reconstruction.

IV. DISCUSSION

In investigating 5-D seismic data interpolation using implicit neural networks, our studies have yielded preliminary results that underscore the potential of this approach. The intrinsic self-regularizing feature of ISR is a promising constraint for inverse problems. By constructing a continuous representation of the data, these networks inherently provide smoothness to the interpolation, thus effectively avoiding overfitting the noise present in the training data. This characteristic is particularly beneficial to seismic data interpolation, where the trade-off between accuracy and generalizability is paramount.

Nevertheless, we must confront the limitations evident in our examples. A primary concern is the insufficient

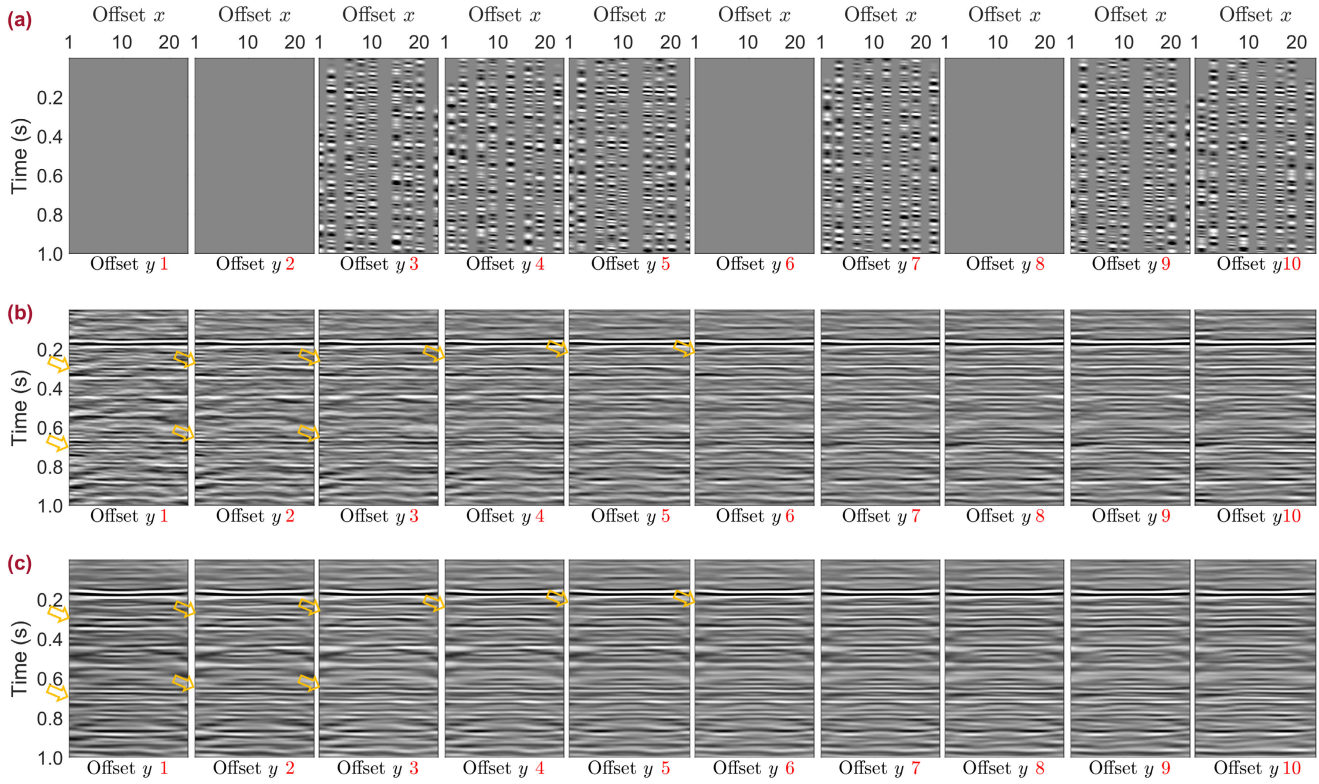


Fig. 5. Slice view of CMP gather results by assigning offset CMP $x = 5$ and CMP y number = 5. (a) Raw data. (b) Reconstructed by DRR. (c) Reconstructed by the proposed ISR method.

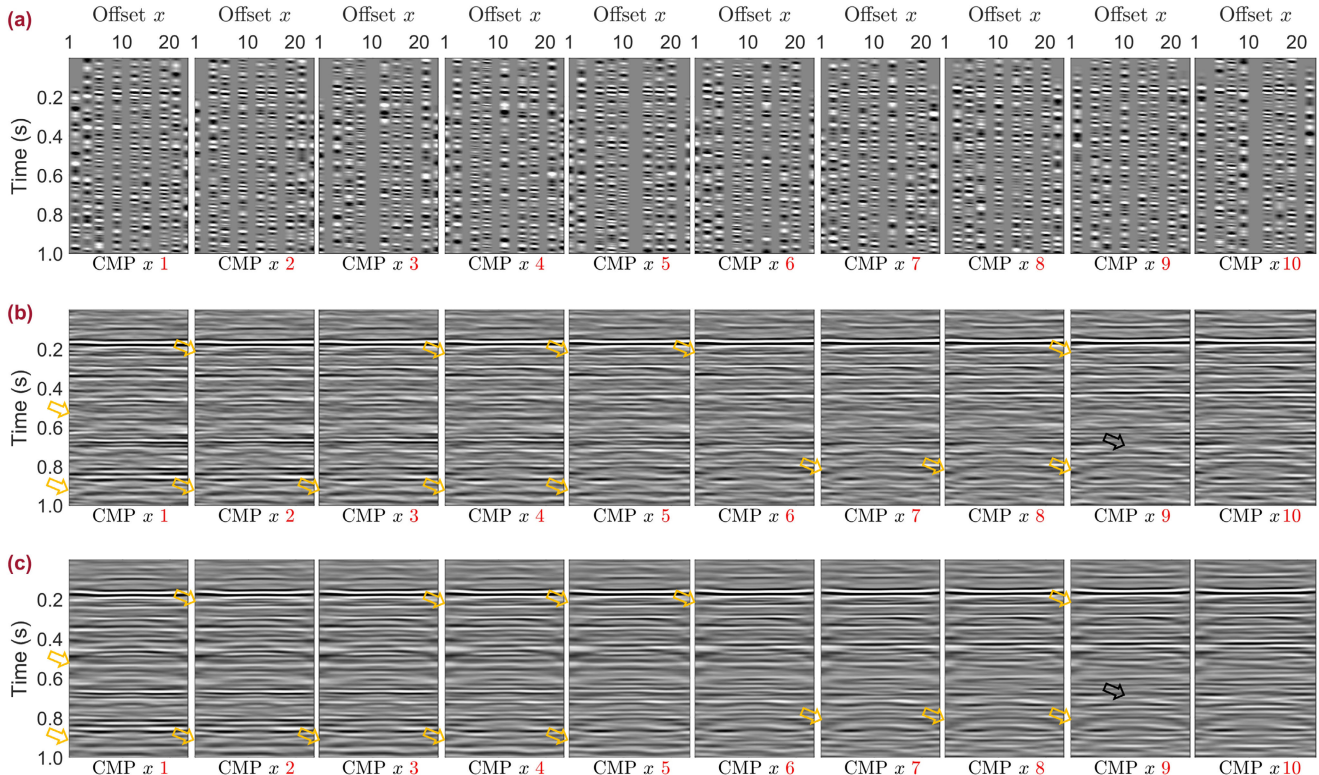


Fig. 6. Slice view of CMP y gather results by assigning CMP y number = 5 and offset y number = 5. (a) Raw data. (b) Reconstructed by DRR. (c) Reconstructed by the proposed ISR method.

denoising capability of the existing ISR framework. Although the network excels at interpolating missing traces, its noise

suppression performance falls short of real-world application requirements. Addressing this deficiency, future enhancements

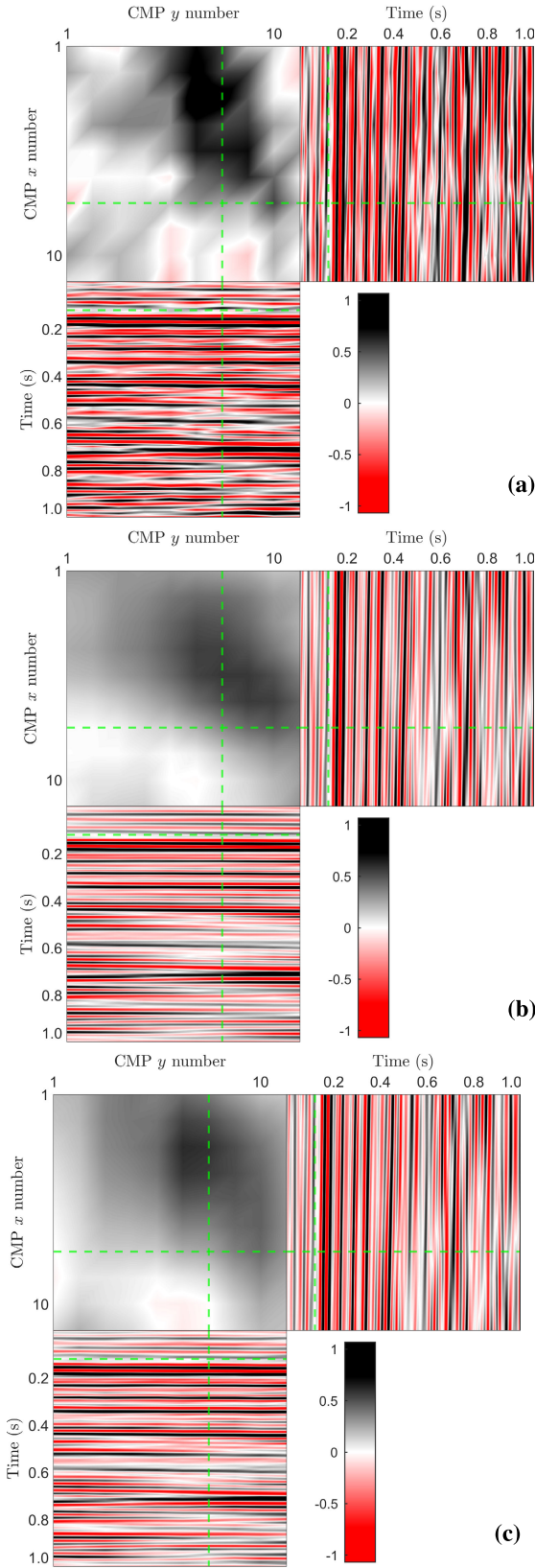


Fig. 7. Stacked results. (a) Before reconstruction. (b) After reconstruction using the DRR method. (c) After reconstruction using the ISR method.

could include integrating established regularization techniques from seismic processing, such as nuclear-norm regularization [61] or total variation regularization [62]. In addition, incorporating a Huber loss function offers a viable pathway

to counteract erratic noise [63]. These strategies are known to effectively reduce noise by inducing sparsity constraints or imposing penalties on solution variability. By embedding these methods into the network's loss function, we expect to significantly bolster its ability to combat intricate noise features typical of field data. Another limitation in our current examples is the focus on regularly sampled data, a constraint dictated by data availability. It is evident, however, that ISR should be equipped to process irregularly sampled data directly by ingesting the original trace coordinates. In addition, the datasets utilized in our experiments are relatively small. They are employed, because they are open-source and widely used for benchmark tests within our academic community. While useful for preliminary assessments, these datasets do not fully demonstrate the superior capability of our method in characterizing global features compared with traditional methods. Since our ISR method uses coordinates as input, the increased dataset size does not constrain network training, because we employ stochastic gradient descent. In forthcoming studies [64], we will test larger datasets, which we believe hold considerable potential for more thoroughly exploring and validating the distinct advantages of our approach.

Despite these limitations, the proposed reconstruction network marginally outperforms conventional methods unsupervised without significantly increasing computation costs. This accomplishment is noteworthy, given the complexity of the task. Moreover, the network architecture provides a versatile backbone for future irregular and complicated reconstructions. The network's inherent flexibility allows for adding task-specific modules, catering to particular reconstruction needs. For instance, one could integrate modules that target specific noise types or enforce geological constraints.

V. CONCLUSION

We have explored the frontier of 5-D seismic data interpolation through implicit neural networks. The implicit neural networks possess self-regularizing characteristics to mitigate the risk of overfitting noisy data. Leveraging this, the proposed ISR interpolation method efficiently fits observed 5-D seismic data points and encodes a continuous 5-D wavefield into an MLP network, offering a novel and computationally efficient representation of seismic data. As a result, the network adeptly interpolates missing data by querying their coordinates. While our implicit neural network approach to 5-D seismic interpolation shows promise over conventional rank-reduction methods, it is still in its nascent stage. Its challenges, particularly in noise suppression, signal fertile ground for further research. Integrating established regularization techniques into the network's architecture could significantly enhance its performance in real-world seismic data processing, paving the way for a more robust and sophisticated tool in the field.

REFERENCES

- [1] Y. Zhou, J. Gao, W. Chen, and P. Frossard, "Seismic simultaneous source separation via patchwise sparse representation," *IEEE Trans. Geosci. Remote Sens.*, vol. 54, no. 9, pp. 5271–5284, Sep. 2016.
- [2] D. Liu, L. Gao, X. Wang, and W. Chen, "A dictionary learning method with atom splitting for seismic footprint suppression," *Geophysics*, vol. 86, no. 6, pp. V509–V523, Nov. 2021.

- [3] D. Liu, W. Wang, X. Wang, Z. Shi, M. D. Sacchi, and W. Chen, "Improving sparse representation with deep learning: A workflow for separating strong background interference," *Geophysics*, vol. 88, no. 1, pp. WA253–WA266, 2022.
- [4] H. L. Taylor, S. C. Banks, and J. F. McCoy, "Deconvolution with the L_1 norm," *Geophysics*, vol. 44, no. 1, pp. 39–52, 1979.
- [5] D. Liu, W. Niu, X. Wang, M. D. Sacchi, W. Chen, and C. Wang, "Improving vertical resolution of vintage seismic data by a weakly supervised method based on cycle generative adversarial network," *Geophysics*, vol. 88, no. 6, pp. V445–V458, Nov. 2023.
- [6] X. Wu, L. Liang, Y. Shi, and S. Fomel, "FaultSeg3D: Using synthetic data sets to train an end-to-end convolutional neural network for 3D seismic fault segmentation," *Geophysics*, vol. 84, no. 3, pp. IM35–IM45, May 2019.
- [7] S. Spitz, "Seismic trace interpolation in the F-X domain," *Geophysics*, vol. 56, no. 6, pp. 785–794, Jun. 1991.
- [8] M. J. Porsani, "Seismic trace interpolation using half-step prediction filters," *Geophysics*, vol. 64, no. 5, pp. 1461–1467, Sep. 1999.
- [9] M. Naghizadeh and M. D. Sacchi, "F-x adaptive seismic-trace interpolation," *Geophysics*, vol. 74, no. 1, pp. V9–V16, Jan. 2009.
- [10] S. Crawley, R. Clapp, and J. Claerbout, "Interpolation with smoothly nonstationary prediction-error filters," in *Proc. SEG Tech. Program Expanded Abstr.*, Jan. 1999, pp. 1154–1157.
- [11] N. Gulunay and R. E. Chambers, "Unaliased F-K domain trace interpolation (UFKI)," in *SEG Technical Program Expanded Abstracts 1996*. Society of Exploration Geophysicists, 1996, pp. 1461–1464, doi: [10.1190/1.1826390](https://doi.org/10.1190/1.1826390).
- [12] V. Bardan, "Trace interpolation in seismic data processing," *Geophys. Prospecting*, vol. 35, no. 4, pp. 343–358, May 1987.
- [13] M. M. N. Kabir and D. J. Verschuur, "Restoration of missing offsets by parabolic radon transform," *Geophys. Prospecting*, vol. 43, no. 3, pp. 347–368, Apr. 1995.
- [14] W. Chen, L. Yang, H. Wang, and Y. Chen, "Fast high-resolution hyperbolic radon transform," *IEEE Trans. Geosci. Remote Sens.*, vol. 60, 2022, Art. no. 4504410.
- [15] J. Liu, G. Liu, and Y. Chou, "Seismic data reconstruction via complex shearlet transform and block coordinate relaxation," *J. Seismic Explor.*, vol. 28, no. 4, pp. 307–332, Feb. 2019.
- [16] S. Fomel and Y. Liu, "Seislet transform and seislet frame," *Geophysics*, vol. 75, no. 3, pp. V25–V38, May 2010, doi: [10.1190/1.3380591](https://doi.org/10.1190/1.3380591).
- [17] S. Gan, S. Wang, Y. Chen, Y. Zhang, and Z. Jin, "Dealiasing seismic data interpolation using seislet transform with low-frequency constraint," *IEEE Geosci. Remote Sens. Lett.*, vol. 12, no. 10, pp. 2150–2154, Oct. 2015.
- [18] G. Hennenfent, L. Fenelon, and F. J. Herrmann, "Nonequispaced curvelet transform for seismic data reconstruction: A sparsity-promoting approach," *Geophysics*, vol. 75, no. 6, pp. WB203–WB210, Nov. 2010.
- [19] R. Shahidi, G. Tang, J. Ma, and F. J. Herrmann, "Application of randomized sampling schemes to curvelet-based sparsity-promoting seismic data recovery," *Geophys. Prospecting*, vol. 61, no. 5, pp. 973–997, Sep. 2013.
- [20] B. Wang, X. Chen, J. Li, and J. Cao, "An improved weighted projection onto convex sets method for seismic data interpolation and denoising," *IEEE J. Sel. Topics Appl. Earth Observ. Remote Sens.*, vol. 9, no. 1, pp. 228–235, Jan. 2016.
- [21] D. Liu, W. Wang, X. Wang, C. Wang, J. Pei, and W. Chen, "Poststack seismic data denoising based on 3-D convolutional neural network," *IEEE Trans. Geosci. Remote Sens.*, vol. 58, no. 3, pp. 1598–1629, Mar. 2020.
- [22] B. Wang, N. Zhang, W. Lu, and J. Wang, "Deep-learning-based seismic data interpolation: A preliminary result," *Geophysics*, vol. 84, no. 1, pp. V11–V20, Jan. 2019.
- [23] Y. Chen, S. Yu, and J. Ma, "A POCS-Net for 3D seismic data interpolation," *Geophysics*, vol. 88, no. 3, pp. 1–100, Dec. 2023.
- [24] H. Kaur, N. Pham, and S. Fomel, "Seismic data interpolation using CycleGAN," in *Proc. SEG Ann. Meeting*, Aug. 2019, pp. 2202–2206.
- [25] F. Qian, Z. Liu, Y. Wang, S. Liao, S. Pan, and G. Hu, "DTAE: Deep tensor autoencoder for 3-D seismic data interpolation," *IEEE Trans. Geosci. Remote Sens.*, vol. 60, 2022, Art. no. 5904219.
- [26] W. Fang, L. Fu, W. Xu, A. Bian, and H. Li, "CCNet-5D: 5D convolutional neural network for seismic data interpolation," *Geophysics*, vol. 88, no. 4, pp. V333–V344, Jul. 2023.
- [27] M. J. Park, J. Jennings, B. Clapp, and B. Biondi, "Seismic data interpolation using a POCS-guided deep image prior," in *Proc. SEG Ann. Meeting*, Sep. 2020, pp. 3154–3158.
- [28] D. Liu, X. Yang, X. Wang, H. Mao, M. D. Sacchi, and W. Chen, "Deep learning for prestack strong scattered noise suppression," in *Proc. 1st Int. Meeting Appl. Geosci. Energy Expanded Abstr.*, Sep. 2021, pp. 1601–1605.
- [29] S. Li et al., "Masked modeling for self-supervised representation learning on vision and beyond," 2024, [arXiv:2401.00897](https://arxiv.org/abs/2401.00897).
- [30] T. He, B. Wu, and X. Zhu, "Seismic data consecutively missing trace interpolation based on multistage neural network training process," *IEEE Geosci. Remote Sens. Lett.*, vol. 19, pp. 1–5, 2021.
- [31] P. Yuan et al., "Self-supervised learning for anti-aliasing seismic data interpolation," in *Proc. 1st Int. Meeting Appl. Geosci. Energy Expanded Abstr.*, Sep. 2021, pp. 1500–1504.
- [32] W. Fang, L. Fu, M. Wu, J. Yue, and H. Li, "Irregularly sampled seismic data interpolation with self-supervised learning," *Geophysics*, vol. 88, no. 3, pp. V175–V185, May 2023.
- [33] K. Zhang, G. Riegler, N. Snavely, and V. Koltun, "NeRF++: Analyzing and improving neural radiance fields," 2020, [arXiv:2010.07492](https://arxiv.org/abs/2010.07492).
- [34] Z. Li, M. Wang, H. Pi, K. Xu, J. Mei, and Y. Liu, "E-NeRV: Expedite neural video representation with disentangled spatial-temporal context," in *Proc. Eur. Conf. Comput. Vis.*, 2022, pp. 267–284.
- [35] Z. Zheng, D. Wu, R. Lu, F. Lu, G. Chen, and C. Jiang, "NeuralPCN: Spatio-temporal neural field for 3D point cloud multi-frame non-linear interpolation," in *Proc. IEEE/CVF Conf. Comput. Vis. Pattern Recognit. (CVPR)*, Vancouver, BC, Canada, Jun. 2023, pp. 909–918.
- [36] M. Debbagh, "Neural radiance fields (NeRFs): A review and some recent developments," 2023, [arXiv:2305.00375](https://arxiv.org/abs/2305.00375).
- [37] D. Trad, "Five-dimensional interpolation: Recovering from acquisition constraints," *GEOPHYSICS*, vol. 74, no. 6, pp. V123–V132, Nov. 2009.
- [38] R. Martin-Brualla, N. Radwan, M. S. Sajjadi, J. T. Barron, A. Dosovitskiy, and D. Duckworth, "NeRF in the wild: Neural radiance fields for unconstrained photo collections," in *Proc. IEEE/CVF Conf. Comput. Vis. Pattern Recognit.*, Jun. 2021, pp. 7210–7219.
- [39] F. Pistilli, D. Valsesia, G. Fracastoro, and E. Magli, "Signal compression via neural implicit representations," in *Proc. IEEE Int. Conf. Acoust., Speech Signal Process. (ICASSP)*, May 2022, pp. 3733–3737.
- [40] K. Wadhani and T. Kojima, "SqueezeNeRF: Further factorized Fast-NeRF for memory-efficient inference," in *Proc. IEEE/CVF Conf. Comput. Vis. Pattern Recognit. Workshops (CVPRW)*, Jun. 2022, pp. 2716–2724.
- [41] Y. Strümpler, J. Postels, R. Yang, L. V. Gool, and F. Tombari, "Implicit neural representations for image compression," in *Eur. Conf. Comput. Vis.*, Oct. 2022, pp. 74–91.
- [42] E. Dupont, H. Kim, S. A. Eslami, D. J. Rezende, and D. Rosenbaum, "From data to functa: Your data point is a function and you can treat it like one," in *Proc. Int. Conf. Mach. Learn.*, 2022, pp. 5694–5725.
- [43] I. Mehta, M. Gharbi, C. Barnes, E. Shechtman, R. Ramamoorthi, and M. Chandraker, "Modulated periodic activations for generalizable local functional representations," in *Proc. IEEE/CVF Int. Conf. Comput. Vis. (ICCV)*, Oct. 2021, pp. 14194–14203.
- [44] Y. Luo, X. Zhao, and D. Meng, "Revisiting nonlocal self-similarity from continuous representation," 2024, [arXiv:2401.00708](https://arxiv.org/abs/2401.00708).
- [45] S. Geman, E. Bienenstock, and R. Doursat, "Neural networks and the bias/variance dilemma," *Neural Comput.*, vol. 4, no. 1, pp. 1–58, Jan. 1992.
- [46] A. M. Saxe, J. L. McClelland, and S. Ganguli, "Exact solutions to the nonlinear dynamics of learning in deep linear neural networks," 2013, [arXiv:1312.6120](https://arxiv.org/abs/1312.6120).
- [47] S. Arora, N. Cohen, W. Hu, and Y. Luo, "Implicit regularization in deep matrix factorization," in *Proc. Adv. Neural Inf. Process. Syst.*, vol. 32. Red Hook, NY, USA: Curran Associates, 2019, pp. 1–11.
- [48] Z. Li, Y. Luo, and K. Lyu, "Towards resolving the implicit bias of gradient descent for matrix factorization: Greedy low-rank learning," 2021, [arXiv:2012.09839](https://arxiv.org/abs/2012.09839).
- [49] N. Razin, A. Maman, and N. Cohen, "Implicit regularization in tensor factorization," 2021, [arXiv:2102.09972](https://arxiv.org/abs/2102.09972).
- [50] G. Gidel, F. Bach, and S. Lacoste-Julien, "Implicit regularization of discrete gradient dynamics in linear neural networks," in *Proc. Adv. Neural Inf. Process. Syst.*, vol. 32, 2019, pp. 1–11.
- [51] D. Gissin, S. Shalev-Shwartz, and A. Daniely, "The implicit bias of depth: How incremental learning drives generalization," 2019, [arXiv:1909.12051](https://arxiv.org/abs/1909.12051).
- [52] N. Razin and N. Cohen, "Implicit regularization in deep learning may not be explainable by norms," in *Proc. Adv. Neural Inf. Process. Syst.*, vol. 33, 2020, pp. 21174–21187.

- [53] N. Rahaman et al., "On the spectral bias of neural networks," in *Proc. Int. Conf. Mach. Learn.*, 2019, pp. 5301–5310.
- [54] Y. Cao, Z. Fang, Y. Wu, D.-X. Zhou, and Q. Gu, "Towards understanding the spectral bias of deep learning," 2019, *arXiv:1912.01198*.
- [55] Z.-Q. J. Xu, Y. Zhang, and T. Luo, "Overview frequency principle/spectral bias in deep learning," 2022, *arXiv:2201.07395*.
- [56] G. Valle-Pérez, C. Q. Camargo, and A. A. Louis, "Deep learning generalizes because the parameter-function map is biased towards simple functions," 2019, *arXiv:1805.08522*.
- [57] M. Tancik et al., "Fourier features let networks learn high frequency functions in low dimensional domains," in *Proc. Adv. Neural Inf. Process. Syst.*, vol. 33, 2020, pp. 7537–7547.
- [58] A. Zaeemzadeh, N. Rahnavaud, and M. Shah, "Norm-preservation: Why residual networks can become extremely deep?" *IEEE Trans. Pattern Anal. Mach. Intell.*, vol. 43, no. 11, pp. 3980–3990, Nov. 2021.
- [59] D. Wu, Y. Wang, S.-T. Xia, J. Bailey, and X. Ma, "Skip connections matter: On the transferability of adversarial examples generated with ResNets," 2020, *arXiv:2002.05990*.
- [60] Y. Chen et al., "Simultaneous denoising and reconstruction of 5-D seismic data via damped rank-reduction method," *Geophys. J. Int.*, vol. 206, no. 3, pp. 1695–1717, May 2016.
- [61] N. Kreimer, A. Stanton, and M. D. Sacchi, "Tensor completion based on nuclear norm minimization for 5D seismic data reconstruction," *Geophysics*, vol. 78, no. 6, pp. V273–V284, Nov. 2013.
- [62] L. I. Rudin, S. Osher, and E. Fatemi, "Nonlinear total variation based noise removal algorithms," *Phys. D, Nonlinear Phenomena*, vol. 60, nos. 1–4, pp. 259–268, 1992.
- [63] P. J. Huber, *Robust Statistics*, vol. 523. Hoboken, NJ, USA: Wiley, 2004.
- [64] J. Li, D. Liu, D. Trad, and M. Sacchi, "Robust unsupervised 5D seismic data reconstruction on both regular and irregular grid," *Geophysics*, vol. 89, no. 6, pp. 1–86, 2024.



Dawei Liu received the bachelor's degree in communication engineering from Chang'an University, Xi'an, China, in 2013, the master's degree in electronic and communication engineering from Xi'an Jiaotong University (XJTU), Xi'an, in 2018, and the Ph.D. degree from the School of Information and Communication Engineering, Xi'an Jiaotong University, in 2022.

He was a Post-Doctoral Scholar with Purdue University, West Lafayette, IN, USA, from 2022 to 2023. He is currently a Post-Doctoral Fellow with the University of Alberta, Edmonton, AB, Canada. His research interests include tensor decomposition, deep learning, and time-frequency analysis and their applications in the seismic data processing.

Dr. Liu is a reviewer of IEEE TRANSACTIONS ON GEOSCIENCE AND REMOTE SENSING, *Geophysics*, *Acta Geophysica*, and *Petroleum Science*.



Wenbin Gao received the bachelor's degree in communication engineering from Jilin University, Changchun, China, in 2021. He is currently pursuing the master's degree in electronic and communication engineering with Xi'an Jiaotong University (XJTU), Xi'an, China.

His research interests include deep learning, and time-frequency analysis and their applications in seismic data processing.



Weiwei Xu received the bachelor's degree in communication engineering from Sichuan University, Chengdu, China, in 2017. He is currently pursuing the Ph.D. degree with the School of Information and Communication Engineering, Xi'an Jiaotong University, Xi'an, China.

From November 2021 to November 2023, he served as a Visiting Scholar at the Image and Sound Processing Lab (ISPL), Politecnico di Milano, Milan, Italy. His research interests include seismic signal processing and machine learning.



Ji Li received the bachelor's and master's degrees in geophysics from the University of Alberta, Edmonton, AB, Canada, in 2018 and 2021, respectively. He is currently pursuing the Ph.D. degree in geoscience with the University of Calgary, Calgary, AB, Canada.

His research interests include robust seismic denoising and interpolation. In addition, he is actively involved in exploring the application of unsupervised deep learning methods to tackle various challenges in seismic data processing.



Xiaokai Wang (Member, IEEE) received the bachelor's degree in information engineering and the Ph.D. degree in communication engineering from Xi'an Jiaotong University (XJTU), Xi'an, China, in 2006 and 2012, respectively.

From 2012 to 2014, he was a Post-Doctoral Fellow with the Institute of Geology and Geophysics, Chinese Academy of Sciences, Beijing, China. He joined the Department of Computational Geophysics, XJTU, in 2015, where he was transferred to the School of Information and Communication Engineering, in 2018. He was a Visitor of the Bureau of Economic Geology, The University of Texas at Austin, Austin, TX, USA, from 2016 to 2017. His research interests include seismic attributes extraction, and time-frequency analysis and their applications in seismic data processing.



Wenchao Chen received the B.S. and M.S. degrees in seismic exploration and information technology from Chang'an University, Xi'an, China, in 1993 and 1996, respectively, and the Ph.D. degree in electromagnetic field and microwave technology from Xi'an Jiaotong University, Xi'an, in 2000.

From 2000 to 2002, he was a Post-Doctoral Fellow with the Department of Computation Science, Northwestern Polytechnical University, Xi'an. Since 2002, he has been with the School of Information and Communications Engineering, Xi'an Jiaotong

University, where he is currently a Professor. His research interests include seismic and ground-penetrating radar (GPR) signal processing, blind signal processing, and sparse representation.

Dr. Chen has served as a member for the Society of Exploration Geophysicists (SEG) and the Chinese Geophysical Society. He is also a referee for several journals, including the IEEE JOURNAL OF SELECTED TOPICS IN APPLIED EARTH OBSERVATIONS AND REMOTE SENSING, IEEE TRANSACTIONS ON GEOSCIENCE AND REMOTE SENSING, *Geophysics*, *Interpretations*, and *Journal of Applied Geophysics*.